

III-V Compound Detectors for CO₂ DIAL Measurements

Tamer F. Refaat¹, M. Nurul Abedin², Oleg V. Sulima³, Syed Ismail² and Upendra N. Singh²

¹ Science and Technology Corp., Hampton VA 23681

² NASA Langley Research Center, Hampton VA 23681

³ University of Delaware, Newark, DE, 19716

ABSTRACT

Profiling of atmospheric carbon dioxide (CO₂) is important for understanding the natural carbon cycle on Earth and its influence on global warming and climate change. Differential absorption lidar is a powerful remote sensing technique used for profiling and monitoring atmospheric constituents. Recently there has been an interest to apply this technique, at the 2 μm wavelength, for investigating atmospheric CO₂. This drives the need for high quality detectors at this wavelength. Although 2 μm detectors are commercially available, the quest for a better detector is still on. The detector performance, regarding quantum efficiency, gain and associated noise, affects the DIAL signal-to-noise ratio and background signal, thereby influencing the instrument sensitivity and dynamic range. Detectors based on the III-V based compound materials shows a strong potential for such application.

In this paper the detector requirements for a long range CO₂ DIAL profiles will be discussed. These requirements were compared to newly developed III-V compound infrared detectors. The performance of ternary InGaSb pn junction devices will be presented using different substrates, as well as quaternary InGaAsSb npn structure. The performance study was based on experimental characterization of the devices dark current, spectral response, gain and noise. The final results are compared to the current state-of-the-art InGaAs technology. Npn phototransistor structure showed the best performance, regarding the internal gain and therefore the device signal-to-noise ratio. 2- μm detectivity as high as $3.9 \times 10^{11} \text{ cmHz}^{1/2}/\text{W}$ was obtained at a temperature of -20°C and 4 V bias voltage. This corresponds to a responsivity of 2650 A/W with about 60% quantum efficiency.

Keywords: Atmospheric CO₂, DIAL, IR Detectors, Characterization, InGaAsSb, Phototransistor

1. INTRODUCTION

Carbon dioxide (CO₂) is an important green house gas that directly affects the Earth's climate and global warming¹. Long-term trend of CO₂ in the atmosphere and its seasonal variations are well documented², but the sources and sinks of CO₂ on continental and regional scales are not well understood. Consequently, concentration of CO₂ has been rapidly increased in the atmosphere during the past 100 years, while its global cycle is not completely understood. This drives the need to increase our knowledge of the spatial and temporal distribution of CO₂, which is essential in predicting its future levels and its impact on climate change²⁻³.

Differential absorption lidar (DIAL) is one of the powerful techniques for measuring the distribution of atmospheric species⁴⁻⁵. DIAL is an active remote sensing technique, which relates the atmospheric backscattered radiation, from transmitted laser pulses, to an absorption feature of the investigated atmospheric specie. This leads to the knowledge of the temporal and spatial distribution of that specie with high accuracy with relatively simple inversion methods. Applying the DIAL technique to profile atmospheric CO₂ requires the selection of appropriate wavelength, which would be collocated with strong absorption for the gas with high distinction relative to other atmospheric molecules. Besides, the selection criteria must take into account the technological availability of various transmitter/receiver components, with high reliability at the specified wavelength⁶⁻⁷. The two-micron wavelength has been proven best suited for profiling atmospheric CO₂⁷. Specifically, the 2.05 μm wavelength, where many absorption peaks are distinctive to carbon dioxide⁷⁻⁸.

Quantum detectors are critical components in the DIAL instrument. Located at the receiver end, the detector converts the collected backscattered radiation into electrical signal compatible with processing and storage electronics. Therefore, the quality of the detector directly affects the performance of the DIAL instrument. The detector gain and noise contributes to the system range and accuracy. Being the dominant noise source in the DIAL instrument, the detector affects the system minimum detectable signal and correspondingly the minimum detectable concentration at a certain range. High quality detectors enhance the system requirements in terms of the required laser power, receiver size and cost. These issues point out the need for a detector with high quantum efficiency, narrow spectral bandwidth and low noise. The existence of an internal gain mechanism is a further advantage in such detectors. Avalanche photodiodes (APD) are ideal choice for DIAL application, but they are not commercially available at the 2 μm wavelength.

According to CO_2 DIAL simulations at 2.05 μm , a suitable detector for this application would be an APD with large area (at least 300 μm diameter), 55% quantum efficiency, 2×10^{-14} $\text{W/Hz}^{1/2}$ noise-equivalent-power (NEP) and 2.5 excess-noise-factor⁹. High responsivity, narrow spectral bandwidth and room temperature operation are additional advantages for such a device. III-V compound detectors have proven decent performance at near and mid infrared wavelengths. Specifically for the 2 μm wavelength, commercial InGaAs pin detectors were successful in monitoring atmospheric CO_2 with the DIAL technique¹⁰. In this paper current state-of-the-art III-V detector technology will be presented. This includes a brief discussion about InGaAs and InGaSb ternary detectors and a special focus on InGaAsSb/AlGaAsSb quaternary phototransistors. The performance of these devices will be compared to the CO_2 DIAL requirement.

2. III-V COMPOUND DETECTORS

III-V compound materials are suitable for fabricating optoelectronic devices in the near and mid-infrared wavelength range. Table I summaries the common III-V compounds and the corresponding energy band gap and cut-off wavelengths¹¹⁻¹³. The availability of binary substrates, such as InAs and GaSb, allows the growth of multilayer homo and hetero-structures, where lattice matched ternary and quaternary layers could be tailored to detect wavelengths in the range of 0.8 to 4 μm ¹⁴. Such detectors are useful for several applications, including atmospheric remote sensing. Even binary III-V compound detectors, such as InAs and InSb, indicated reasonable performance in the mid-infrared range. Commercially, these detectors are available either in a photoconductive or photovoltaic (p-n junction) configuration. They have sensitivity at wavelengths around 2 μm , but they have limited performance. The detectivity (D^*) of these devices can exceed 10^{11} $\text{cmHz}^{1/2}/\text{W}$ only by cooling down to liquid nitrogen temperatures, which increases the complexity of their applied systems¹⁵⁻¹⁶. Out of the binaries, the room temperature cut-off wavelength of GaSb is 1.7 μm (the closest to the 2 μm) making it suitable for 2 μm detector substrates.

Out of the III-V compounds, InGaAs ternary material indicated better performance for 2 μm applications. With D^* close to 10^{12} $\text{cmHz}^{1/2}/\text{W}$ and area diameter as large as 3 mm, InGaAs pin detectors proof success in measuring atmospheric CO_2 using DIAL^{10, 17-18}. Also they are commercially available in the form of linear arrays and APD with performance that match or exceed mature Ge APD technology¹⁹⁻²⁰. A shortcoming of InGaAs APD arises due to the shorter cut-off wavelength of 1.8 μm . On the other hand, InGaSb ternary material indicated good performance for 2 μm detectors²¹, but still they are on the research level not being commercially available. The availability of ternary InGaSb virtual substrates has a promising potential for developing high performance detectors at wavelengths around the 2 μm , without the influence of the binary substrates usually used for processing the ternary materials²².

Quaternary III-V compound materials are excellent candidate for 2 μm detection. Several articles reported different device structures using materials such as InGaAsSb and AlGaAsSb²³⁻²⁹. Several reports discussed the performance of InGaAsSb APD especially for applications such as optical communication²³⁻²⁶. Such devices usually involve much complicated structures with difficult material processing. Recently, using the same material, a new InGaAsSb/AlGaAsSb phototransistor has been developed²⁷⁻²⁹. Aside from an APD, a phototransistor can achieve higher gain and better signal-noise-ratio, without the excess noise effects, which makes it attractive for 2 μm applications. The performance of these devices has even exceeded the InGaAs pin technology in some areas²⁷⁻²⁹. In the following section we will focus on the characterization results for these new devices and compare their characteristics with state-of-the-art InGaAs and InGaSb devices.

Table I summary of various III-V compound materials and their energy band gap and cut-off wavelengths at room temperature.

Material	Band-Gap	Cut-off Wavelength
	E [eV]	λ [μm]
AlAs	2.95	0.42
AlSb	2.30	0.54
GaP	2.74	0.45
GaAs	1.42	0.87
GaSb	0.72	1.73
InP	1.35	0.92
InAs	0.36	3.45
InSb	0.18	6.9
$\text{In}_x\text{Ga}_{1-x}\text{As}$	0.36 – 1.42	0.87 – 3.45
$\text{In}_x\text{Ga}_{1-x}\text{Sb}$	0.18 – 0.72	1.73 – 6.90
$\text{In}_x\text{Ga}_{1-x}\text{As}_y\text{Sb}_{1-y}$	0.18 – 1.42	0.87 – 6.90
$\text{Al}_x\text{Ga}_{1-x}\text{As}_y\text{Sb}_{1-y}$	0.72 – 2.95	0.42 – 1.73

3. InGaAsSb/AlGaAsSb PHOTOTRANSISTORS

The structure of the newly developed phototransistor is shown in figure 1. Obtained from AstroPower, Inc. the device was grown lattice matched to a GaSb substrate using liquid phase epitaxy. The structure includes an n-type AlGaAsSb emitter, p-type composite base consisting of AlGaAsSb and InGaAsSb layers, and an n-type InGaAsSb collector²⁹. The device area has a total diameter of 400 μm with sensitive area diameter of 200 μm after metallization. No antireflection coating was applied. The performance of the phototransistors is compared to InGaSb detectors obtained from Rensselaer Polytechnic Institute (RPI). InGaSb detector samples were grown on either binary or ternary substrates. The InGaSb/GaSb detectors consist of p-type and n-type epitaxial layers of InGaSb, grown on an n-type binary GaSb substrate²¹. For InGaSb/InGaSb detectors, tellurium doped n-type ternary InGaSb substrates were grown by the vertical Bridgman technique and the p-n devices were fabricated using Zn-diffusion²². Also commercial InGaAs pin detectors, obtained from Hamamatsu, were used for the comparison. All detectors were characterized at NASA Langley Research Center (Table II) using similar operating conditions. The characterization included dark current, spectral response, gain and noise measurements. Special focus is drawn to room temperature results, since it allows the use of simple thermoelectric coolers (TEC) based temperate controller, which further reduce the complexity of the DIAL instrument.

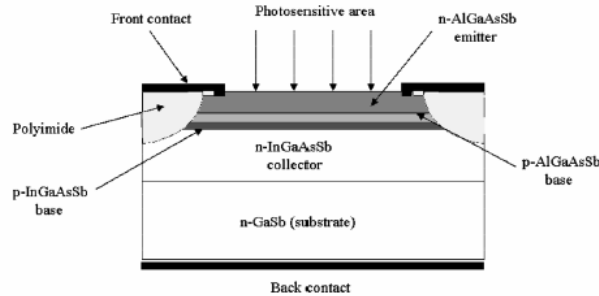


Figure 1 Schematic of the npn phototransistor structure grown on n-GaSb substrate.

Table II Summary of the different detectors considered in this study.

Detector	Manufacturer	Size	Structure
InGaAs(2.3)	Hamamatsu (G5852)	1.0 mm diameter	pin photodetector
InGaAs(2.6)	Hamamatsu (G5853)	1.0 mm diameter	pin photodetector
InGaSb/GaSb	RPI	0.8 mm diameter	pn photodetector
InGaSb/InGaSb	RPI	300x300 μm^2	pn photodetector
A1-a2, -b1, -b3, -c3, -d2	AstroPower, Inc.	200 μm diameter	nnp phototransistor

3.1 Dark Current Measurement

Assuming two terminal devices, dark current measurements were obtained by measuring the device current-voltage (I-V) characteristics at dark conditions. The I-V characteristics were measured in a temperature controlled environment using a Semiconductor Characterization System (Keithley, 4200), with 10 mV steps and 20 mA maximum current limit. Figure 2(a) shows the dark current density variation with bias voltage for different phototransistor samples, compared to InGaAs pin detectors. Dark current density of the phototransistors is 3 orders of magnitude higher than that of the pin detector. This is expected due to the different device structures. With the phototransistor, I-V measures the emitter current versus collector-emitter voltage, which is normally high. To the DIAL point of view this might be of serious concern due to the fact of higher power consumption operating these devices. Biasing the phototransistor at a fixed voltage level consumes a certain “dark power” regardless of the incident optical signal. Added to this fact the direct relation between the noise and dark current of a detector, higher noise contents for the phototransistor would be expected compared to the pin detectors. This leads to the necessity of cooling down the devices. Generally, cooling a detector reduces its dark current and associated noise, but affects its sensitivity and increases the complexity of the related electronics.

Figure 2(b) shows the dark current variation with bias voltage for one of the phototransistor samples at different temperatures. Absence of any intersection in the characteristics indicates that there is no avalanche gain. This confirms the transistor action of the device. It is also noticeable that the temperature dependence of the dark current changes with the bias voltage. At low temperatures, dark current has strong temperature dependence at bias voltages lower than about -1.5V . Similar response is observed at higher temperatures. At bias voltages higher than -1.5V the temperature has much less influence on the dark current. This might be attributed to the nature of the dark current dominating each region. Generally, At lower bias, diffusion and generation-recombination currents are dominant and both of these components are highly temperature dependent. At higher bias voltage the tunneling current becomes dominant, which has much weaker temperature dependence³⁰.

One advantage of the new phototransistor is that it survives very high temperature deviations. Phototransistor samples tested at temperatures up to 120°C and down to 80 K indicate the potential of these devices for severe operating conditions. Although the performance is affected, the results were reproducible for each setting without damage or performance deterioration³¹.

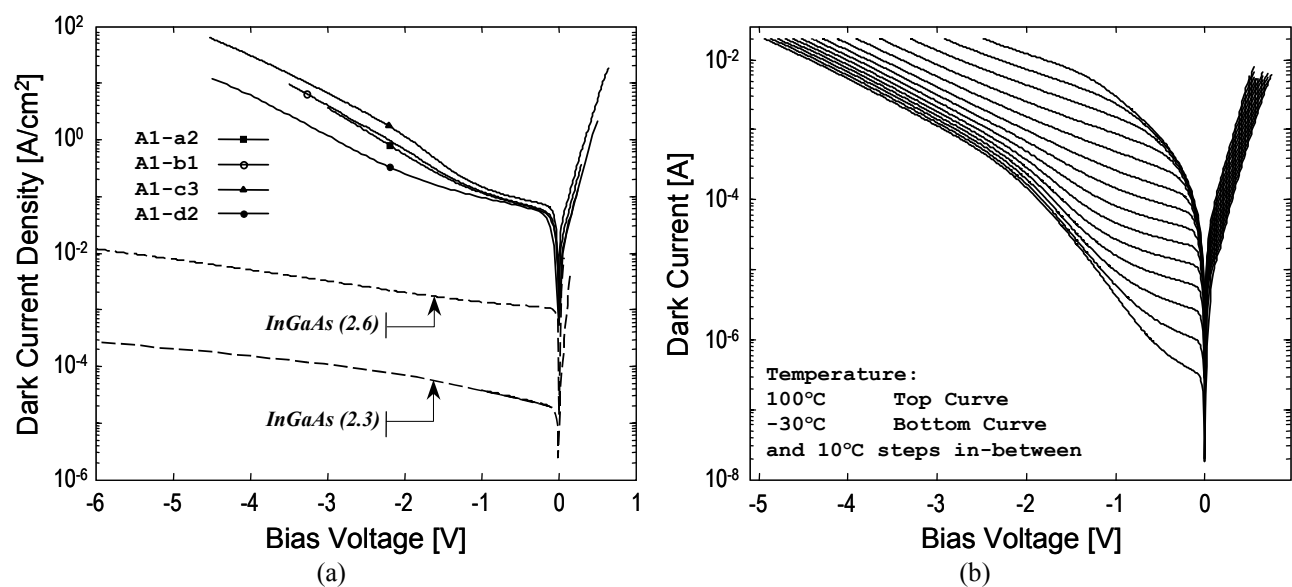


Figure 2 I-V characteristics at 20°C for different phototransistor samples, compared to InGaAs pin detectors (a), and at different temperatures for sample A1-c3 (b).

3.2 Spectral Response Measurement

The spectral response of a detector defines its responsivity variation with the wavelength of the incident radiation. To achieve the spectral response of the tested samples, the devices were calibrated using the substitution method, in reference to a calibrated 3x3 mm² PbS detector³². The PbS detector spectral calibration range spans from 1 to 3.2 μm . For shorter wavelengths, a calibrated 10 mm diameter Si detector was used. All of the samples were calibrated in similar operating conditions to insure minimal uncertainties in the comparison. Figure 3 shows the spectral response calibration results for the different samples along with constant quantum efficiency contours. The results were obtained at 20°C operating temperature and 0 V bias voltage. Background signal was minimized by placing the samples in a dark enclosure. The calibrated radiation source inlet was set at 20 and 40 nm resolutions for the phototransistor samples and the other samples, respectively.

InGaAs detectors with 2.3 and 2.6 μm cut-off showed better 2 μm response. The highest responsivity of 1.15 A/W was achieved by the InGaAs(2.6) pin detector. The spectral response of the InGaSb/GaSb sample reveals two distinctive peaks. The peak locations are at about 1.7 and 2 μm corresponding to the band gaps of the GaSb substrate and the In_xGa_{1-x}Sb (x= 0.2) epitaxial layers, respectively as indicated in Table I. For the InGaSb/InGaSb sample, the peak shifts to about 1.9 μm due to the slight deviation in the indium composition (x=0.17). Although replacing the substrate of the InGaSb detector indicated lower responsivity, it enhances the dark current and the overall noise contents of the device⁸. Shown in the same figure the spectral response of two phototransistor samples. These results indicate the maximum and minimum responsivities obtained from all the phototransistor samples. The phototransistor indicated responsivity enhancement around the 2.0 μm wavelength with cut-off at 2.2 μm . Reduced responsivity was observed at wavelengths shorter than 1.8 μm , down to 0.5 μm , with another shorter peak observed at 0.85 μm . The reduction in the responsivity at wavelengths shorter than 1.8 has the advantage of reducing the background signal, which increases the detector dynamic range for the DIAL return signal. Besides, this might lower the restriction regarding the narrow band pass filter requirements for the DIAL detection.

Generally, the responsivity, \mathcal{R} , of a detector is a function of the incident radiation wavelength, λ , and the bias voltage, V , and the temperature, T , of the device. Therefore, if the detector has an output current, I_s , which corresponds to an incident optical power P , the responsivity is expressed as

$$\mathcal{R}(\lambda, T, V) = \frac{I_s(\lambda, T, V)}{P} = \frac{q}{h \cdot c} \cdot G(V, T) \cdot \eta(\lambda, T) \cdot \lambda \quad (1)$$

where q , h , c are the electron charge, Plank's constant and speed of light respectively, G is the device gain and η is the quantum efficiency. Here we assume that the gain has higher bias voltage dependence, with a unity value at zero bias voltage, and any wavelength dependence is neglected. This is a valid assumption, since the gain involves amplification of the generated charge carriers rather than the absorbed photons. On the other hand, the quantum efficiency, defined as the probability of generating an electron-hole pair (charge carriers) for each photon incident on the detector surface, is mainly dependent on the optical properties of the material system used. Therefore it will have higher temperature and wavelength dependence while the bias voltage dependence can be neglected. A general relation for the quantum efficiency can be expressed in the form

$$\eta(\lambda, T) = (1 - R(\lambda, T)) \cdot (1 - e^{-\alpha(\lambda, T)L}) \cdot \xi \quad (2)$$

where R is the normal incident reflection coefficient, α in the absorption coefficient and ξ is a factor dependent on the recombination processes³³. The assumptions of the gain and quantum efficiency dependences are the only way to separate both quantities from equation (1).

Focusing on the phototransistor samples, figure 4 shows the variation of the spectral response with temperature, obtained at 0 V bias voltage. Due to the temperature dependence of the bandgap, the cut-off wavelength shifts to a shorter value at lower temperatures. This might cause the loss of the 2 μm sensitivity, as indicated in figure 4(a) for the cryogenic temperature curve. Spectral response enhancement is observed, by an increase in the longer wavelength responsivity at lower temperature. The responsivity enhancement might be due to the improvement of the recombination

process at lower temperatures. For a specific wavelength, an optimum operating temperature can be defined by observing the responsivity variation with temperature, which maximizes the quantum efficiency of the device; since 0V bias is used in this case (i.e. the responsivity is directly proportional to the quantum efficiency). This is shown in figure 5 corresponding to the 2.05 μm line in figure 4 and other samples. Although different samples have different optimum temperature dependencies, it was noticeable that the optimum temperature for maximum quantum efficiency lies in the -20°C temperature range. This is easily achievable by using simple TEC based temperature controller, rather than complicated cryogenic systems. This temperature range has direct influence on the cost and complexity of the CO₂ DIAL system.

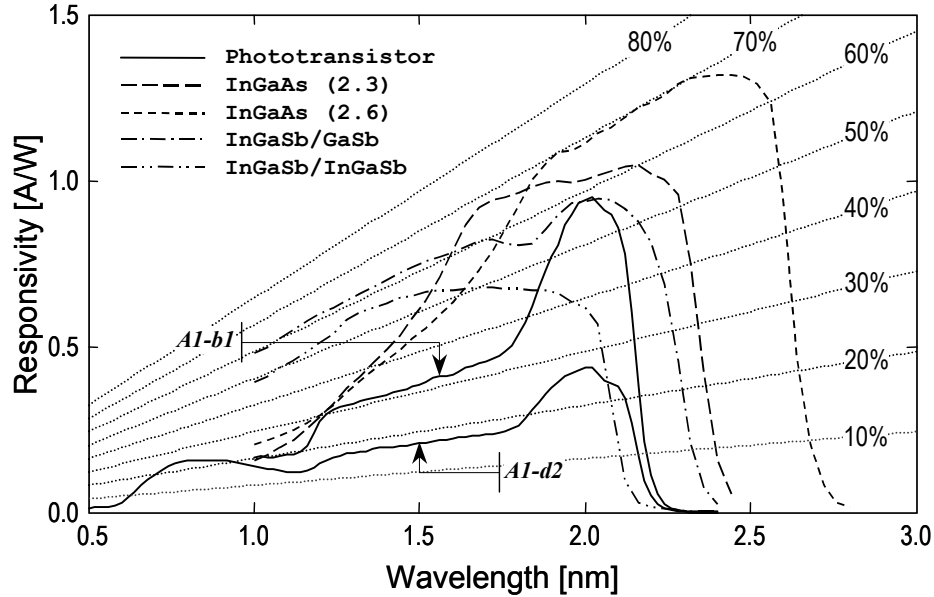


Figure 3 Spectral response and quantum efficiency for different 2 μm detector samples at 0 V bias and 20°C.

Investigating higher bias voltage operation, figure 6 shows the spectral response variation with bias voltage at the specified temperatures for different samples. At a fixed temperature, increasing the bias voltage increases the responsivity of the phototransistor. Experimentally, bias voltage is limited to the current carrying capacity of the device as determined by the I-V measurements (current limit of 20 mA). Examining figure 6(a), for sample A1-c3 at 20°C, it is noticeable that the spectral response profile changes at higher bias voltage compared to the 0V one, especially at shorter wavelength. This indicates some voltage dependence of the quantum efficiency, probably at the recombination term (equation (2)). Surface recombination might be affected by the bias voltage, which dominates the shorter wavelength. Responsivity as high as 569.7 A/W was achieved by this sample at 4 V bias and 2.05 μm as shown in figure 6(a). Cooling down the same sample to -16.5°C, which is the optimum operating temperature according to figure 5, the responsivity increases to 825.8 A/W as indicated in figure 6(b). Additionally, cooling reduces the dark current, according to figure 2(b). This results in increasing the signal-to-noise ratio of the device. Examining the extreme limit of the device, figure 6(c) shows the same characteristics for sample A1-d2 at 50°C. It is interesting to observe the sudden increase in the responsivity at lower bias voltage. More interesting is the comparison of the spectral response at cryogenic temperature at zero bias voltage (figure 4(a) and figure 6(d)) and higher bias voltage given in figure 6(d). Although there is almost zero quantum efficiency and negligible responsivity at the 2.05 μm wavelength, 80.1K and 0V, as indicated in the figure, increasing the bias voltage up to 5V regains the 2.05 μm responsivity to 177.4 A/W. At this temperature and bias voltage level, responsivities as high as 2.2×10^4 A/W is detected at 1.84 μm .

3.3 Responsivity and Gain Variations at 2 μm

At a certain bias voltage, V , the phototransistor gain can be obtained by comparing the responsivity at that bias level to the responsivity at zero bias voltage. According to equation (1), the phototransistor gain is given by

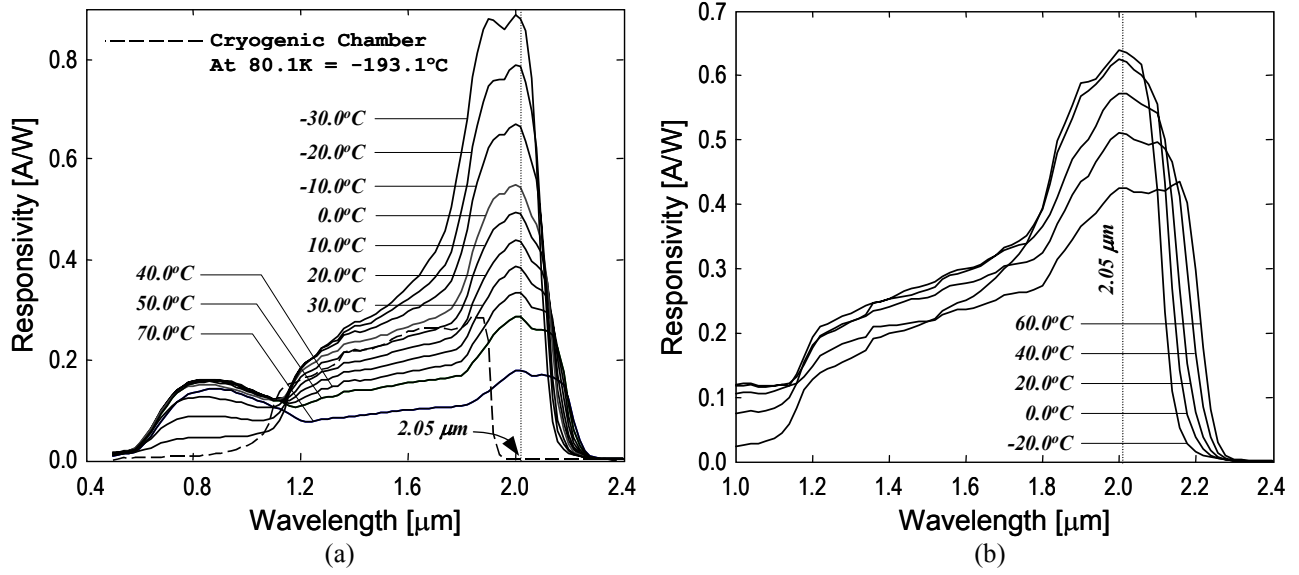


Figure 4 Spectral response variation with temperature for the phototransistor samples A1-d2 (a) and A1-c3 (b) at 0V bias. The A1-d2 sample was also tested at 80.1K.

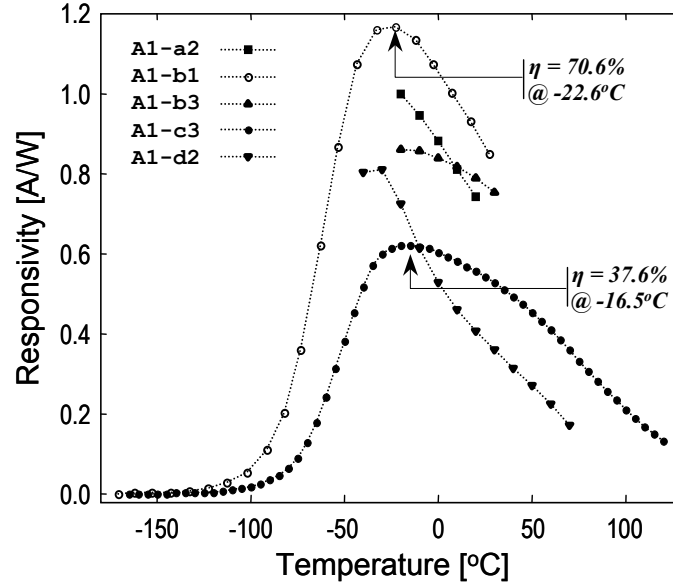


Figure 5 Responsivity variation with temperature at 0 V bias for different phototransistor samples. The curve indicates the optimum operating temperature to achieve maximum quantum efficiency.

$$G(V) = \frac{\Re(V)}{\Re(0)} \Big|_{T, \lambda} \quad (3)$$

This relative measurement is important to determine the optimum bias voltage operation. Experimentally, this measurement is obtained by dividing the detector output current with a bias voltage to that without bias at fixed operating condition in terms of temperature wavelength and radiation intensity. This is accomplished after eliminating the dark current component, by modulating the input optical radiation. The intensity level is important in this measurement since it is necessary to avoid the device nonlinearity.

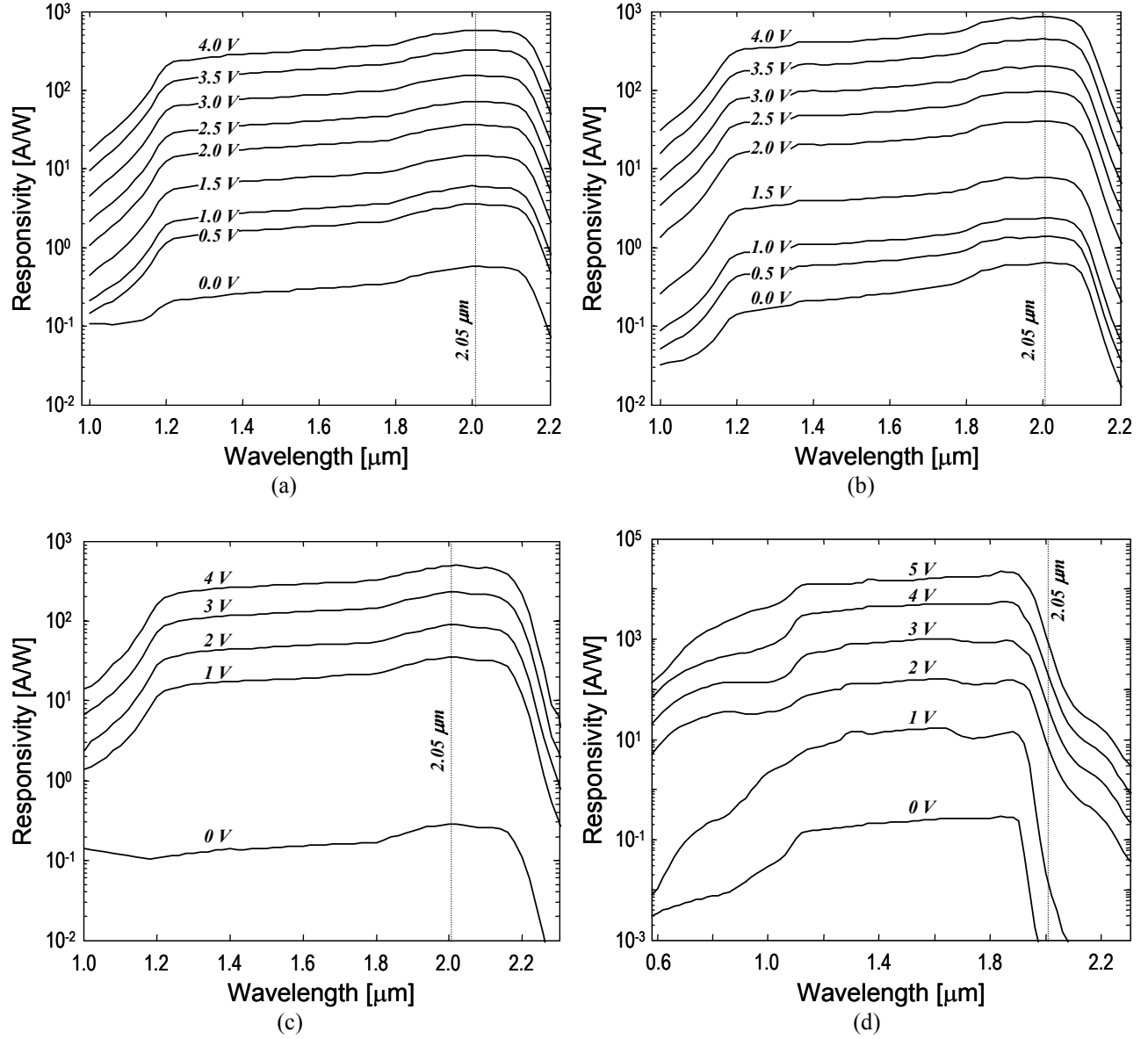


Figure 6 Spectral response variation with bias voltage for sample A1-c3 at (a) 20.0°C and (b) -16.5°C and for sample A1-d2 at (c) 50°C and (d) 80.1K.

Figure 7 shows the gain variation with bias voltage obtained at fixed temperature and 2.05 μm wavelength. Note that the data of the curves coincides with the vertical lines, marked 2.05 μm , in figure 6. Sharp increase in the gain is observed at 20°C at low bias voltage, as shown in figure 7(a). This is followed by a parabolic increase in the gain until the device saturates. This behavior is common for all the samples. For most of the phototransistor samples, cooling down the device leads to increase the gain, and gives a higher margin to increase the bias voltage due to the reduction in the dark current, as indicated in figure 7(b).

Although InGaAs pin detectors should not have an internal gain, biasing these devices showed a slight increase in the output signal. This is probably due to the increase of the space charge region at higher bias leading to increase the absorption regions of the devices. Nevertheless, higher voltage operation of the device enhances both the output signal and the bandwidth.

Figure 8(a) shows the gain variation with bias voltage for sample A1-d2 at four different temperatures. Sharp increase in the gain is noticeable at low bias voltages at high temperatures. At 80.1 K the same sharp response is observed with a huge of gain, reaching a maximum of 3.8×10^5 at 5V. Although the gain is extremely high, it is of no use, due to the deterioration of the quantum efficiency that destroys the responsivity at the wavelength of interest at these operating conditions. Finally, figure 8(b) shows the responsivity variation with temperature at three different bias voltages at 2 μm . Again, at lower temperatures and zero bias we observe very low responsivity. But at higher voltages, due to the high gain, the device regains its sensitivity.

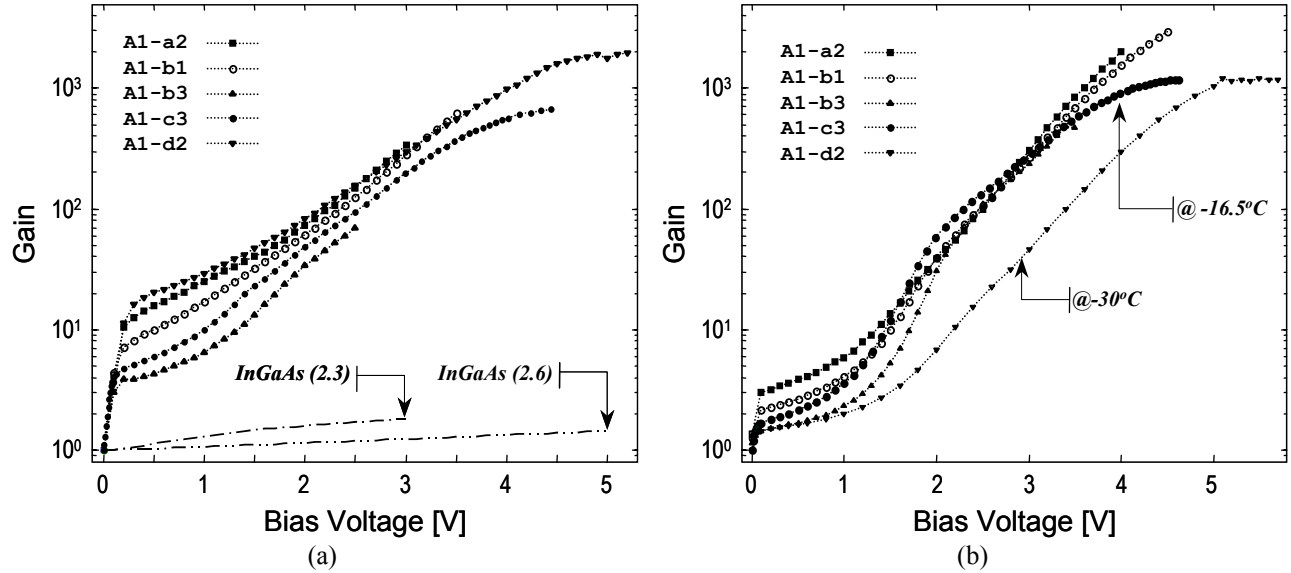


Figure 7 Gain variation with bias voltage, obtained at 2.05 μm wavelength and 20°C for different phototransistor and pin detector samples (a) and at -20°C (b) for different phototransistor samples.

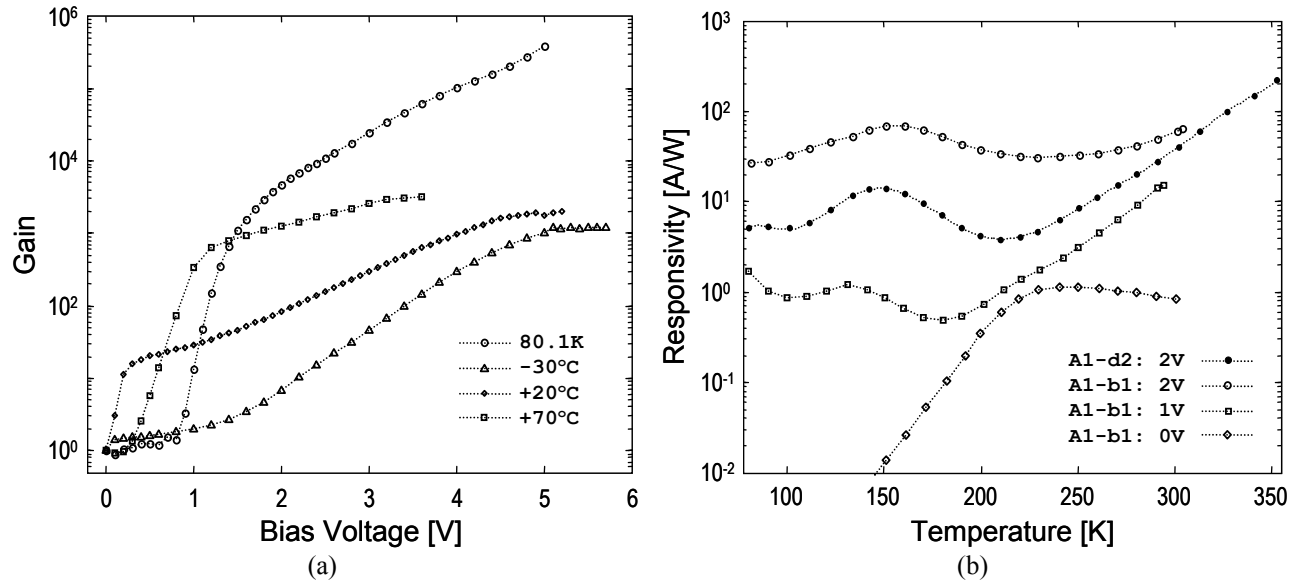


Figure 8 Gain variation with bias voltage at 2.05 μm for sample A1-d2 at different temperatures (a) and responsivity variation with temperature at 2.05 μm at different bias voltages for samples A1-b1 and A1-d2 (b).

3.4 Noise Measurement

The noise spectral density was measured for the detector samples in dark condition at fixed operating conditions. At a certain temperature and bias voltage setting, the noise voltage spectral density of a test detector was measured in conjunction with the preamplifier (Stanford Research Systems; SR570) using a spectrum analyzer (Stanford Research Systems; SR785) in the frequency band 0 Hz to 100 kHz, with 1-Hz normalization and 50-kHz center frequency. The noise spectrum was averaged 4000 times, and the mean value was calculated in the operating frequency band. The preamplifier noise current was measured associated with the setup and with the detector replaced by a short circuit. The net detector noise was then calculated by subtracting the preamplifier and setup noise from the total noise measured with the detector. The noise voltage was then converted to the noise current spectral density using the amplifier gain setting.

For the InGaAsSb phototransistors, noise increases rapidly with increasing device temperature and bias voltage. Figure 9(a) shows the variation of the noise current spectral density with bias voltage obtained at 20 °C. Generally the noise level is fixed at lower bias voltage and then increase rapidly up to a level at which it tends to saturate. Shown on the same figure, the noise variation for the InGaAs samples. InGaAs provides less noise, even with larger area. Cooling down the phototransistor reduces the noise as indicated in figure 9(b). This is proportional to the dark current variation with temperature observed in figure 2. Detectivity analysis indicated values as high as $3.9 \times 10^{11} \text{ cmHz}^{1/2}/\text{W}$, which was obtained at a temperature of -20°C and 4 V bias at $2 \text{ } \mu\text{m}^2$. Detectivity as high as $10^{13} \text{ cmHz}^{1/2}/\text{W}$ detectivity was also achieved with A1-a2 sample at a temperature of 80.2K and 5 V bias around $1.7 \text{ } \mu\text{m}$ wavelength³⁴.

3.5 Capacitance Measurement

The detector capacitance is a combination of different type of capacitance associated with its operation. The depletion region (space charge region) capacitance is one of the dominant capacitances that limits the device bandwidth. The capacitance measurement relies on the variation of that capacitance with the applied bias voltage. Figure 10 shows the variation of the InGaAs pin detector and a phototransistor sample capacitance and its variation with bias voltage. The capacitance was measured using Precision LCR Meter (Hewlett Packard 4285A) at 1 MHz base frequency and 10 mV amplitude, while the device was placed in controlled temperature environment. The InGaAs results were compared to the manufacturer data sheet as indicated in the figure. This result indicates a capacitance of 80 pF corresponding to a 40 MHz bandwidth, satisfying the bandwidth-capacitance relation

$$BW = 1/100 \cdot \pi \cdot C \quad (4)$$

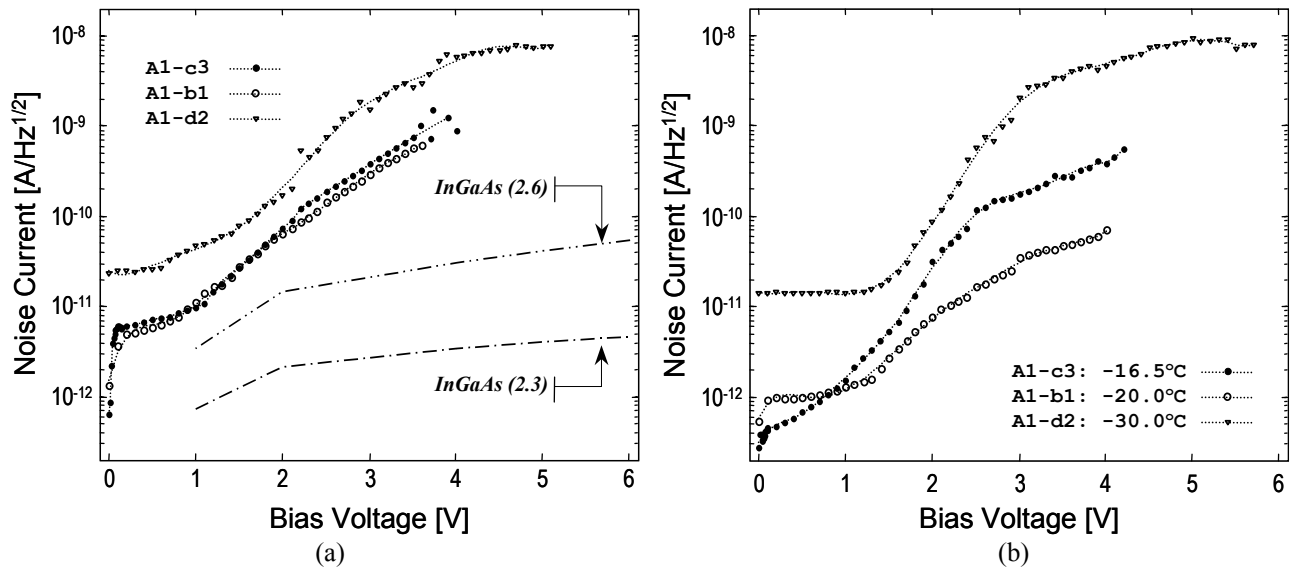


Figure 9 Noise current variation with bias voltage obtained at dark conditions for different samples at 20°C (a) and different low temperatures (b).

where BW is the bandwidth and C is the capacitance. This equation assumes a typical $50\ \Omega$ terminating resistance. Following the same criteria, the phototransistor bandwidth is 150 and 260 MHz, corresponding to capacitances of 21.2 and 12.3 pF, obtained at -0.7 and -1.7 V at temperatures of 20 and -20°C , respectively. These results matches previously reported results on similar device using different bandwidth measurement technique²⁸.

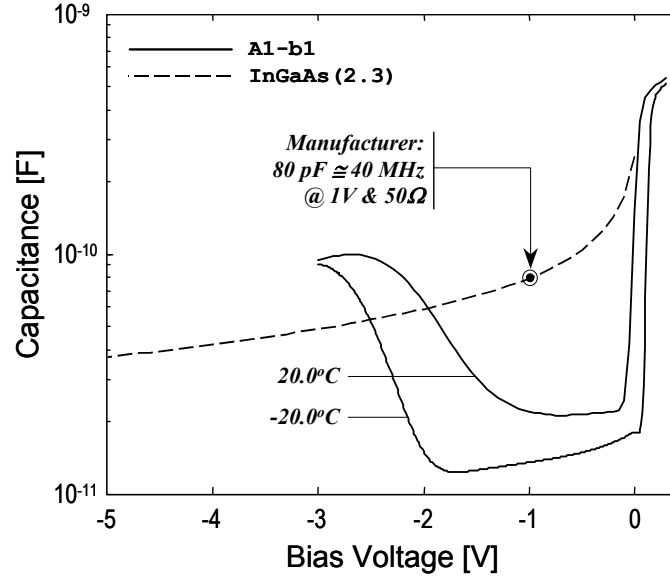


Figure 10 Capacitance-Voltage characteristics for InGaAs pin and phototransistor samples in dark condition with 1 MHz and 10 mV excitation.

4. SUMMARY AND CONCLUSION

In this paper a review of III-V compound detectors was presented. A special focus was toward a newly developed InGaAsSb phototransistor. The devices are optimized for 2- μm applications and exhibit high gain at low operating bias voltage. I-V measurements indicated higher dark current associated with the operation of these devices compared to other III-V compound detectors. Dark current measurements reveal the absence of avalanche gain. Although high dark current leads to increase the device power consumption and noise, enhanced signal-to-noise ratio is observed due to the high internal gain. Several samples were tested at temperatures up to 120°C and down to -193°C (80K) with high reliability and without any damage or performance deterioration. Spectral response measurements indicated responsivity enhancement around the 2 μm wavelength, with a cut-on at 1.8 μm and cut-off at 2.2 μm . The devices are sensitive to wavelengths as low as 0.6 μm . The reduction in the responsivity at wavelengths shorter than 1.8 μm has the advantage of reducing the background signal, leading to increase the system dynamic rang. Responsivity as high as 2650 A/W corresponding to an internal gain of 2737 has been measured with -4.4 V bias voltage at -20°C . Maximum quantum efficiency was achievable at 2 μm by optimizing the operating temperature. It was noticeable that the optimum temperature for maximum quantum efficiency lies in the -20°C range, which is easily achievable using simpler and lower cost TEC based temperature controller. Higher bias voltage operation leads to increase the dark current, gain and noise. The optimum bias voltage can be obtained by maximizing either the device gain or signal-to-noise ratio (D^*). Noise measurements resulted in $3.9 \times 10^{11} \text{ cmHz}^{1/2}/\text{W}$ detectivity at 2 μm . This is equivalent to $4.5 \times 10^{-14} \text{ W/Hz}^{1/2}$ NEP, which is close to the CO₂ DIAL requirement. Capacitance measurements indicated strong dependence on both bias voltage and temperature. These measurements led to bandwidth estimation of 150 and 260 MHz, corresponding to capacitances of 21.2 and 12.3 pF, obtained at -0.7 and -1.7 V with temperatures of 20 and -20°C , respectively. Application of this device for 2- μm CO₂ DIAL system should be attempted.

Acknowledgement

This effort is part of the Laser Risk Reduction Program funded by NASA's Earth Science Technology Office and NASA's Enabling Concepts & Technologies Program. The authors would like to thank George Komar and Chris Moore for their continues support. Thanks also due to Prof. Ishwara B. Bhat for his valuable discussions regarding InGaSb detectors.

References

1. R. Christopherson, *Geosystems, an Introduction to physical Geography*, Macmillan Publishing Company, New York, 1992.
2. C. Keeling, "Atmospheric carbon dioxide variations at Mauna Loa Observatory Hawaii", *Tellus*, **26**(6), 538-551, 1976.
3. J. Kaiser and K. Schmidt, "Coming to grips with the world's greenhouse gases", *Science*, **281**, 504-506, 1998.
4. E. Browell, S. Ismail and S. Shipley, "Ultraviolet DIAL measurements of O₃ profiles in regions of spatially inhomogeneous aerosols", *Applied Optics*, **24**(17), 2827-2836, 1985.
5. N. Higdon, E. Browell, P. Ponsardin, B. Grossmann, C. Butler, T. Chyba, M. Mayo, R. Allen, A. Heuser, W. Grant, S. Ismail, S. Mayor and A. Carter, "Airborne differential absorption lidar system for measurements of atmospheric water vapor and aerosols", *Applied Optics*, **33**(27), 6422-6438, 1994.
6. G. Koch, M. Petros, J. Yu and U. Singh, "Precise wavelength control of single-frequency pulsed Ho:Tm:YLF laser", *Applied Optics*, **41**(9), 1718-1721, 2002.
7. P. Ambrico, A. Amodeo, P. Girolamo and N. Spinelli, "Sensitivity analysis of differential absorption lidar measurements in the mid-infrared region", *Applied Optics*, **39**(36), 6847-6865, 2000.
8. T. Refaat, N. Abedin, G. Koch, S. Ismail & U. Singh, "Infrared detectors characterization for CO₂ DIAL measurements", *Proceeding of SPIE*, **5154**, 65-73, 2003.
9. S. Ismail, G. Koch, E. Browell, U. Singh, N. Abedin, J. Yu and J. Hair, "A 2-micron DIAL system for profiling atmospheric CO₂", *21st International Laser Radar Conference*, Quebec City, Canada, 2002.
10. M. Uchiumi, N. Vasa, M. Fujiwara, S. Yokoyama, M. Maeda and O. Uchino, "development of DIAL for CO₂ and CH₄ in the atmosphere", *Proceeding of SPIE*, **4893**, 141-149, 2003.
11. S. Adachi, "Dielectric functions and optical parameters of Si, Ge, GaP, GaAs, GaSb, InP, InAs and InSb from 1.5 to 6.0 eV", *Physical Review B*, **27**(2), 985-1009, 1983.
12. S. Adachi, "Model dielectric constants of GaP, GaAs, GaSb, InP, InAs, and InSb", *Physical Review B*, **35**(14), 7454-7463, 1987.
13. S. Adachi, "Optical dispersion relations for GaP, GaAs, GaSb, InP, InAs, InSb, Al_xGa_{1-x}As and In_{1-x}Ga_xAs_yP_{1-y}", *Journal of Applied Physics*, **66**(12), 6030-6040, 1989.
14. I. Bhat, Y. Xiao, V. Bhagwath, P. Dutta, T. Refaat and N. Abedin, "GaInAsSb-based IR detectors in the 2 μ m range fabricated from layer structures grown by metalorganic vapor phase epitaxy", *Military Sensing Symposia MSS*, 2005.
15. J12D Series InAs Detectors Operating Instructions, Judson Technologies, PB220, October, 2000.
16. J10D Series InSb Detectors Operating Instructions, Judson Technologies, PB211, August, 2000.
17. InGaAs PIN photodiode G8422/G8372/G5852 series, Data Sheet, Hamamatsu, October, 2004.
18. InGaAs PIN photodiode G8423/G8373/G5853 series, Data Sheet, Hamamatsu, March, 2005.
19. C30645E/C30662E Series InGaAs Avalanche Photodiode, Data Sheet, PerkinElmer, 2004.
20. T. Martin and P. Dixon, "InGaAs sees infrared and visible light", *Laser Focus World*, **40**(11), 2004.
21. T. Refaat and N. Abedin, I. Bhat, P. Dutta & U. Singh, "Characterization of InGaSb/GaSb p-n photodetectors in the 1.0- to 2.4- μ m wavelength range", *Optical Engineering*, **43**(5), 1014-1015, 2004.
22. T. Refaat, N. Abedin, V. Bhagwat, I. Bhat, P. Dutta & U. Singh, "InGaSb photodetectors using an InGaSb substrate for 2- μ m applications", *Applied Physics Letters*, **85**(11), 1874-1876, 2004.
23. M. Mikhailova, I. Andreev, A. Baranov, S. Mel'nikov, Y. Smortchkova and Y. Yakovlev, "Low-noise GaInAsSb/GaAlAsSb SAM avalanche photodiode in the 1.6-2.5 μ m spectral range", *Proceedings of SPIE*, **1580**, 308-312, 1991.
24. I. Andreev, M. Afrailov, A. Baranov, M. Mirsagatov, M. Mikhailov, and Y. Yakovlev, "GaInAsSb/GaAlAsSb avalanche photodiode with separate absorption and multiplication regions. *Soviet Technical Physics Letters*, 435-437, 1988.

25. J. Benoit, M. Boulou, G. Soulage, A. Joullie, and H. Mani, "Performance evaluation of GaAlAsSb/GaInAsSb SAM-APDs for high bit rate transmission in the 2.5 μm wavelength region", *Journal of Optical Communication*, **9**(2), 55-58, 1988.
26. I. Andreev, M. Afrailov, A. Baranov, S. Konnikov, M. Mirsagatov, M. Mikhailova, O. Salata, V. Umanskii, G. Filaretova, and Y. Yakovlev, "Ultrafast GaInAsSb p-i-n photodiode for the spectral interval 1.5-2.3 μm :", *Soviet Technical Physics Letters*, **15**(4), 253-254, 1989.
27. T. F. Refaat and M. N. Abedin, O. V. Sulima, S. Ismail & U. N. Singh, "AlGaAsSb/InGaAsSb phototransistors for 2- μm remote sensing applications", *Optical Engineering*, **43**(7), 1647-1650, 2004.
28. O. Sulima, T. Refaat, M. Mauk, J. Cox, J. Li, S. Lohokare, M. Abedin, U. Singh & J. Rand, "AlGaAsSb/InGaAsSb phototransistors for spectral range around 2 μm ", *Electronics Letters*, **40**(12), 766-767, 2004.
29. N. Abedin, T. Refaat, O. Sulima and U. Singh, "AlGaAsSb/InGaAsSb heterojunction phototransistor with high optical gain and wide dynamic range", *IEEE Transaction on Electron Devices*, **51**(12), 2013-2018, 2004.
30. S. Forrest, "Performance of InGaAsP photodiodes with dark current limited by diffusion, generation, recombination and tunneling", *IEEE Journal of quantum Electronics*, **QE-17**(2), 217-226, 1981.
31. N. Abedin, T. Refaat and U. Singh, "Recent development of Sb-based phototransistors in the 0.9- to 2.2 μm wavelength range for applications to laser remote sensing", *Workshop on Frontiers in Electronics (WOFE-04)*, 2004.
32. T. Larason, S. Bruce, and A. Parr, "Spectroradiometric detector measurements: part I ultraviolet detectors and part II visible to near-infrared detectors", *NIST Special Publications*, 250-41, 1998.
33. B. Saleh and M. Tiech, *Fundamentals of Photonics*, John Wiley & Sons, Inc., 1991.
34. T. Refaat, N. Abedin, O. Sulima, U. Singh and S. Ismail, "Novel infrared phototransistors for atmospheric CO₂ profiling at 2 μm wavelength", *IEEE International Electron Devices Meeting; IEDM Technical Digest*, 355-358, 2004.